A&A 654, L1 (2021)
https://doi.org/10.1051/0004-6361/202141989

Astronomy & Astrophysics

LETTER TO THE EDITOR

First detection of C_2H_5NCO in the ISM and search of other isocyanates towards the G+0.693-0.027 molecular cloud

L. F. Rodríguez-Almeida[1], V. M. Rivilla[1,2], I. Jiménez-Serra[1], M. Melosso[3], L. Colzi[1,2], S. Zeng[4], B. Tercero[5], P. de Vicente[5], S. Martín[6,7], M. A. Requena-Torres[8,9], F. Rico-Villas[1], and J. Martín-Pintado[1]

[1] Centro de Astrobiología (CSIC-INTA), Ctra Ajalvir km 4, 28850 Torrejón de Ardoz, Madrid, Spain
e-mail: lrodriguez@cab.inta-csic.es
[2] INAF-Osservatorio Astrofisico di Arcetri, Largo Enrico Fermi 5, 50125 Florence, Italy
[3] Dipartimento di Chimica "Giacomo Ciamician", Universitá di Bologna, via F. Selmi 2, 40126 Bologna, Italy
[4] Star and Planet Formation Laboratory, Cluster for Pioneering Research, RIKEN, 2-1 Hirosawa, Wako, Saitama 351-0198, Japan
[5] Observatorio de Yebes (IGN), Cerro de la Palera s/n, 19141 Guadalajara, Spain
[6] Eureopean Southern Observatory, Alonso de Córdova 3107, Vitacura 763 0355, Santiago, Chile
[7] Joint ALMA Observatory, Alonso de Córdova 3107, Vitacura 763 0355, Santiago, Chile
[8] University of Maryland, College Park, ND 20742-2421, USA
[9] Department of Physics, Astronomy and Geosciences, Towson University, MD 21252, USA

Received 9 August 2020 / Accepted 13 September 2021

ABSTRACT

Context. Little is known about the chemistry of isocyanates (compounds with the functional group R-N=C=O) in the interstellar medium (ISM), as only four of them have been detected so far: isocyanate radical (NCO), isocyanic acid (HNCO), N-protonated isocyanic acid (H_2NCO^+), and methyl isocyanate (CH_3NCO). The molecular cloud G+0.693-0.027, located in the Galactic Centre, represents an excellent candidate to search for new isocyanates since it exhibits high abundances of the simplest ones, HNCO and CH_3NCO.
Aims. After CH_3NCO, the next most complex isocyanates are ethyl isocyanate (C_2H_5NCO) and vinyl isocyanate (C_2H_3NCO). Their detection in the ISM would enhance our understanding of the formation of these compounds in space.
Methods. We have searched for C_2H_5NCO, H_2NCO^+, C_2H_3NCO, and cyanogen isocyanate (NCNCO) in a sensitive unbiased spectral survey carried out in the 2 mm and 7 mm radio windows using the IRAM 30m and Yebes 40m radio telescopes, respectively.
Results. We have detected C_2H_5NCO and H_2NCO^+ towards G+0.693-0.027 (the former for the first time in the ISM) with molecular abundances of $(4.7–7.3)\times10^{-11}$ and $(1.0–1.5)\times10^{-11}$, respectively. A ratio of $CH_3NCO/C_2H_5NCO = 8\pm1$ is obtained; therefore, the relative abundance determined for HNCO:CH_3NCO:C_2H_5NCO is 1:1/55:1/447, which implies a decrease by more than one order of magnitude, going progressively from HNCO to CH_3NCO and to C_2H_5NCO. This is similar to what has been found for alcohols and thiols, for example, and suggests that C_2H_5NCO is likely formed on the surface of dust grains. In addition, we have obtained column density ratios of HNCO/NCO > 269, HNCO/H_2NCO^+ ~ 2100, and $C_2H_3NCO/C_2H_5NCO < 4$. A comparison of the methyl/ethyl ratios for isocyanates (-NCO), alcohols (-OH), formiates (HCOO-), nitriles (-CN), and thiols (-SH) is performed and shows that ethyl derivatives may be formed more efficiently for the N-bearing molecules than for the O- and S-bearing molecules.

Key words. astrochemistry – ISM: molecules – line: identification

1. Introduction

More than 240 molecules[1] have been detected in the interstellar medium (ISM). Among them, only the following four are carrying the isocyanate functional group (-N=C=O): isocyanic acid (HNCO), one of the first detected molecule in space (Snyder & Buhl 1972); isocyanic radical (NCO) and N-protonated isocyanic acid (H_2NCO^+), only reported in the L483 dense core (Marcelino et al. 2018); and methyl isocyanate (CH_3NCO, hereafter MeNCO), reported in hot cores (e.g., Sgr B2N, Orion KL, G10.47+0.03; Halfen et al. 2015; Cernicharo et al. 2016; Gorai et al. 2020), hot corinos (e.g., IRAS 16293-2422, Serpens SMM1; Ligterink et al. 2017, 2021; Martín-Doménech et al. 2017), and in the G+0.693-0.027 molecular cloud (hereafter G+0.693; Zeng et al. 2018).

[1] https://cdms.astro.uni-koeln.de/classic/molecules

Isocyanates are molecules with prebiotic interest since they play a role in the synthesis of amino acids, the polymerisation of peptides (Pascal et al. 2005), and in the production of nucleotides (Choe 2021) and nucleosides (Schneider et al. 2018). Until now, MeNCO has been the most complex isocyanate detected in the ISM, while the search of more complex species, such as ethyl isocyanate (C_2H_5NCO, hereafter EtNCO), only yielded upper limits (Kolesniková et al. 2018; Colzi et al. 2021).

In this Letter, we describe the detection of EtNCO towards G+0.693. This cloud, located in the Galactic Centre within the Sgr B2 molecular complex, contains a very rich chemical inventory (Requena-Torres et al. 2008; Zeng et al. 2018; Rivilla et al. 2019, 2020, 2021b; Jiménez-Serra et al. 2020; Rodríguez-Almeida et al. 2021). G+0.693 is thought to be undergoing a cloud-cloud collision (Zeng et al. 2020), which produces large-scale shocks that sputter dust grains, enhancing

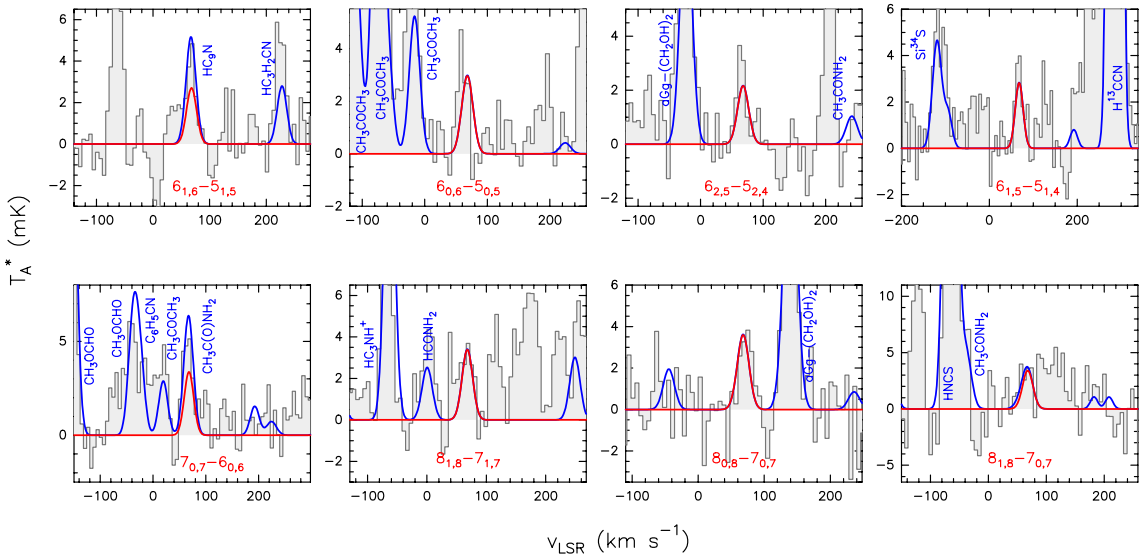

Fig. 1. Selected lines of EtNCO. The grey areas indicate the observed spectra smoothed up to 3 km s^{-1} for optimal line visualisation; while the red and blue lines represent the best LTE fit for the single EtNCO and all the other detected species, respectively. Blue labels indicate the detected species within each spectral range while the quantum numbers of each EtNCO line are indicated in red. See the text and Table 1 for more details.

the gas-phase abundance of molecules by several orders of magnitude (Requena-Torres et al. 2006). Since the abundances of HNCO are MeNCO in this cloud are relatively high (>10^{-10}; Zeng et al. 2018), together with several detections of other ethyl derivatives, such as ethanol (C_2H_5OH, hereafter EtOH; Requena-Torres et al. 2006), ethyl cyanide (C_2H_5CN, hereafter EtCN; Zeng et al. 2018), and recently ethyl mercaptan (C_2H_5SH, hereafter EtSH; Rodríguez-Almeida et al. 2021), G+0.693 represents an excellent candidate for the search of EtNCO and other isocyanates.

2. Observations

A high sensitivity spectral survey was carried out towards G+0.693. We used both the IRAM 30m (Granada, Spain) and Yebes 40m telescopes (Guadalajara, Spain). The observations were centred at α(J2000.0) = 17^{h}47^{m}22^s and δ(J2000.0) = −28°21′27″. The position switching mode was used in all the observations with the off position located at an offset of $\Delta\alpha = -885''$, $\Delta\delta = 290''$. For the IRAM 30m observations, the dual polarisation receiver EMIR was used connected to the fast Fourier transform spectrometers (FFTS), which provided a channel width of 200 kHz in the radio windows from 71.8 to 116.7 GHz and from 124.8 to 175.5 GHz. The observations with the Yebes 40m radiotelescope (project number 20A008, PI Jiménez-Serra) used the Nanocosmos Q-band (7 mm) HEMT receiver (Tercero et al. 2021). The receiver was connected to 16 FFTS, providing a channel width of 38 kHz and a bandwidth of 18.5 GHz per lineal polarisation, covering the frequency range between 31.3 GHz and 50.6 GHz. Readers can refer to Zeng et al. (2020) and Rivilla et al. (2021b) for a more detailed description of the observations.

3. Analysis and results

For the line identification of the molecular species, we used the MADCUBA software[2]. This is supported by the Spectral Line Identification and Modelling (SLIM) tool, which generates synthetic spectra under the assumption of local thermodynamic equilibrium (LTE) conditions and also considering line opacity effects (Martín et al. 2019). The free parameters of the fits are as follows: the column density (N), the excitation temperature (T_{ex}), the full width at half maximum (FWHM), and the local standard of rest velocity (v_{LSR}). For the LTE analysis of each molecular species, we have also considered the emission from other molecules previously identified in our spectral survey that could potentially produce line contamination (Requena-Torres et al. 2006, 2008; Zeng et al. 2018; Rivilla et al. 2019, 2020, 2021b,a; Jiménez-Serra et al. 2020; Rodríguez-Almeida et al. 2021). For each molecule analysed in this work, we have listed the details of the spectroscopy in Appendix A.

3.1. Detection of EtNCO

Figure 1 shows the brightest lines of EtNCO (details of the spectroscopy in Table A.1) detected at levels above 5σ in integrated intensity towards G+0.693, which add up to a total of eight transitions. Five of them appear unblended, while the other three are slightly blended with known (and identified) molecular species (see Table 1). The contamination from unidentified lines is negligible for these transitions, except for the line at 33.966 GHz which shows a small excess with respect to the LTE fit. The remaining lines of EtNCO with line intensities predicted by the LTE fit at levels above 5σ are strongly blended with the emission of other species. It is worth mentioning that all clear transitions have been detected in the 7 mm radio window, which is less affected by line overlaps. The LTE fit was carried out by fixing the FWHM and v_{LSR} to 21 km s^{-1} and 68 km s^{-1}, respectively, giving a $T_{ex} = 10 \pm 2$ K and $N = (8.1 \pm 1.3) \times 10^{12}$ cm^{-2}. To calculate the molecular abundance with respect to H_2 (all the abundances through the text are given with respect to H_2, unless otherwise mentioned), we used $N_{H_2} = 1.35 \times 10^{23}$ cm^{-2} derived by Martín et al. (2008). To estimate the uncertainties of the molecular abundance, we considered the error in the column density obtained with MADCUBA with an additional 15% of uncertainty on account of calibration errors. We obtain a

[2] MADCUBA is a software developed by the Centro de Astrobiología (CSIC-INTA) located in Madrid (Spain). https://cab.inta-csic.es/madcuba/index.html.

Table 1. Spectroscopic and information of the LTE fitting of the selected lines of EtNCO shown in Fig. 1.

Frequency (GHz)	QNs $(J''_{K_a'',K_c''} - J'_{K_a',K_c'})$	E_u (K)	$\log A_{ul}$ (s^{-1})	rms (mK)	$\int T_A^* dv$ (mK km s^{-1}) [a]	S/N [b]	Blending
32.537109	$6_{1,6}-5_{1,5}$	6.0	−5.4198	1.5	61	7	Blended with HC_9N
33.545973	$6_{0,6}-5_{0,5}$	5.7	−5.3818	1.2	67	10	Clean
33.966567	$6_{2,5}-5_{2,4}$	7.9	−5.4239	1.2	49	7	Clean
35.293167	$6_{1,5}-5_{1,4}$	6.5	−5.3498	1.3	63	9	Clean
38.944488	$7_{0,7}-6_{0,6}$	7.5	−5.1881	1.2	76	11	Blended with $CH_3C(O)NH_2$
43.270670	$8_{1,8}-7_{1,7}$	9.9	−5.0473	1.6	76	8	Clean
44.274655	$8_{0,8}-7_{0,7}$	9.7	−5.0220	1.5	82	10	Clean
46.895390	$8_{1,8}-7_{0,7}$	10.7	−5.3581	2.7	77	5	Blended with unidentified species

Notes. The frequency, quantum numbers (QNs), the energy of the upper level (E_u), the logarithm of the Einstein coefficients ($\log A_{ul}$), the root mean square (rms) of the analysed spectral region, the integrated intensity ($\int T_A^* dv$), and the signal-to-noise ratio in integrated intensity (S/N) are given. [a]Integrated intensity derived from MADCUBA LTE fit, see Sect. 3 for details. [b]$S/N = \left(\int T_A^* dv\right) \Big/ \left[\mathrm{rms}\left(\frac{\Delta v}{FWHM}\right)^{0.5} FWHM\right]$, where Δv represents the spectral resolution of the data in velocity units.

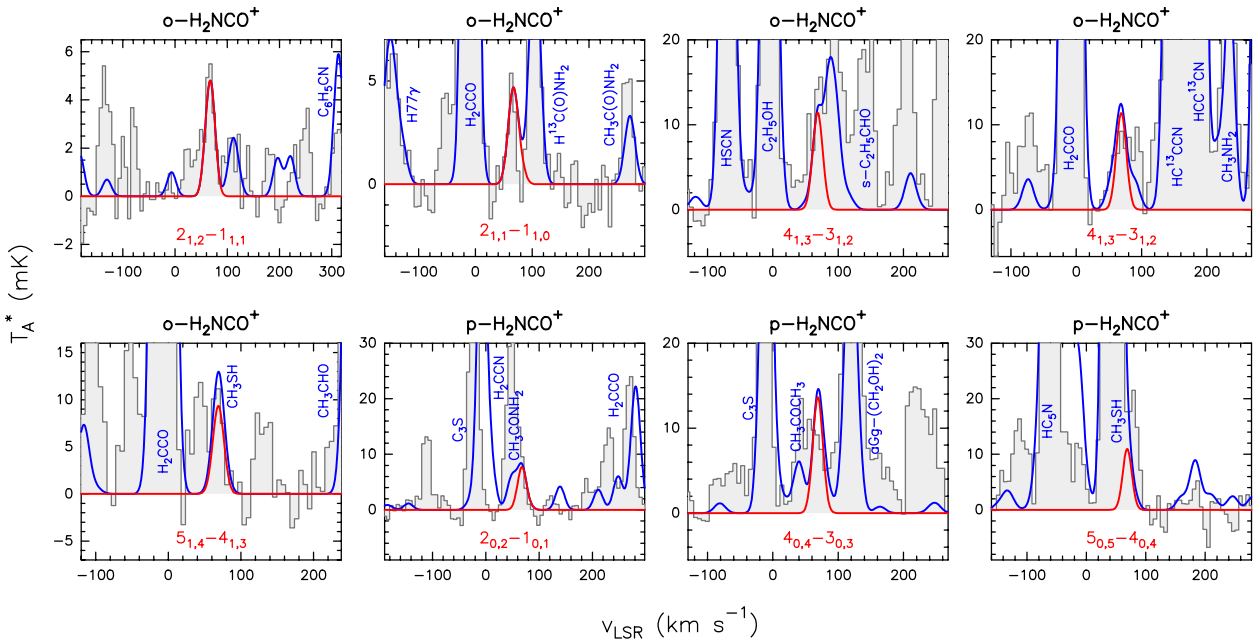

Fig. 2. Selected lines of H_2NCO^+. See Fig. 1 for a description of the information given in the plot. In this case, the LTE fit was carried out separating ortho (o-H_2NCO^+) and para (p-H_2NCO^+) species (see the text for details), which are indicated above each panel. See Table B.1 for a complete description of the quantum numbers.

molecular abundance of $(4.7–7.3)\times10^{-11}$. With the results obtained from EtNCO and the derived column density of MeNCO towards G+0.693 (Zeng et al. 2018), a ratio of MeNCO/EtNCO = 8 ± 1 is obtained.

3.2. Detection of H_2NCO^+ and search for other isocyanates

We note that H_2NCO^+ (see Table A.1 for the spectroscopic references) has been already reported towards L483 (Marcelino et al. 2018) and tentatively detected towards Sgr B2 (Gupta et al. 2013). Since the T_{ex} towards G+0.693 is low, we have separated ortho and para states for the analysis (energy difference ∼15 K; Gupta et al. 2013).

In Fig. 2 and Table B.1, we show the H_2NCO^+ transitions detected towards G+0.693, including the following: six transitions of the ortho state (K_a odd, o-H_2NCO^+), three of which are unblended, and three transitions of the para state (K_a even, p-H_2NCO^+) which appear blended with other species. The LTE fits of the ortho and para states were obtained separately. For o-H_2NCO^+, we fixed v_{LSR} and FWHM at 69 and 18 km s^{-1}, respectively, obtaining $N = (1.1 \pm 0.2)\times10^{12}$ cm^{-2} and $T_{ex} = 7 \pm 1$ K. For the para states, we assumed the same T_{ex} and obtained $N = (6.3 \pm 1.7)\times10^{11}$ cm^{-2}. The total N (ortho + para) gives $(1.7 \pm 0.2)\times10^{12}$ cm^{-2} and an abundance of $(1.1–1.5)\times10^{-11}$ (Fig. 3).

We also searched for other isocyanates, namely the following: isocyanate radical (NCO) – previously found towards L483 (Marcelino et al. 2018) – vinyl isocyanate (C_2H_3NCO), cyanogen isocyanate (NCNCO), and ethynyl isocyanate (HCCNCO) with the references used to search for them listed in Table A.1. Since none of them were detected, a 3σ upper limit to their column densities was measured using the cleanest and brightest transition in the dataset in each case (presented in Appendix C). The derived upper limits are $<1.4\times10^{13}$ cm^{-2}

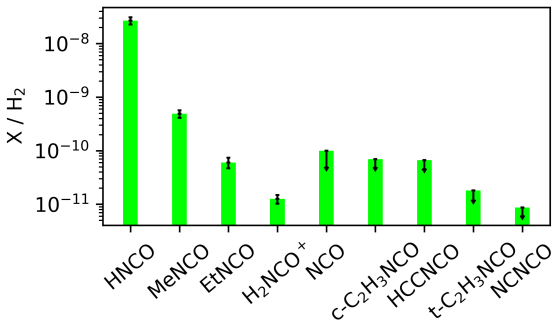

Fig. 3. Molecular abundances with respect to H_2 of the isocyanates targeted towards G+0.693.

for NCO, $<1.2\times10^{12}$ cm^{-2} for NCNCO, $<2.5\times10^{12}$ cm^{-2} for trans-C_2H_3NCO, $<9.3\times10^{12}$ cm^{-2} for cis-C_2H_3NCO, and $<8.9\times10^{12}$ cm^{-2} for HCCNCO (see Table C.1).

4. Discussion

4.1. Isocyanate family in G+0.693

In Fig. 3, we have plotted the abundances of the isocyanates already detected in G+0.693 (HNCO and MeNCO; Zeng et al. 2018) together with the ones reported in this work (detected: EtNCO and H_2NCO^+, and non-detected upper limits: NCO, cis/trans-C_2H_3NCO and NCNCO). Among the detected species, the molecular abundances decrease when increasing the chemical complexity (Fig. 3): HNCO > MeNCO > EtNCO. On the contrary, the simplest species, the radical NCO, is not detected, with an upper limit that is a factor of 5 lower than the abundance of MeNCO. The high reactivity of this radical could explain its low gas-phase abundance.

The ratio of ethyl/vinyl (i.e. EtNCO/C_2H_3NCO) gives >3.7 and >1.5 for the cis and trans isomers of C_2H_3NCO, respectively. This is in contrast with the ethyl/vinyl ratio found towards G+0.693 in cyanides ($C_2H_5NH_2/C_2H_3NH_2$ ~0.7; Zeng et al. 2021).

The ratio H_2NCO^+/HNCO gives $\sim0.5\times10^{-3}$, which is around five times lower than that found towards the cold core L483 of $\sim2.5\times10^{-3}$ (Marcelino et al. 2018). This might indicate that the H_2NCO^+/HNCO ratio decreases with the kinetic temperature of the source (~50–150 K in G+0.693 and ~10 K in L483; Zeng et al. 2018 and Agúndez et al. 2019, respectively). A similar behaviour has been recently observed for the $HCNH^+$/HCN ratio towards a sample of massive star-forming regions, where the ratio varies from 0.1–0.05 in starless (i.e. cold) sources (in agreement with the value found in the low-mass cold core L1544 of ~0.05 to $(1–5)\times10^{-3}$ in protostellar (i.e. hot) sources; Quénard et al. 2017; Fontani et al. 2021, respectively). These authors propose that the distinct values are due to different formation routes of $HCNH^+$ at low and hot temperatures. Further observations of H_2NCO^+ towards new sources and dedicated chemical models (see also Sect. 4.3) are needed to understand how the H_2NCO^+/HNCO ratio varies with the gas temperature.

4.2. Methyl-to-ethyl ratios in the ISM

The detection of EtNCO in the ISM, and the recent confirmation of EtSH (Rodríguez-Almeida et al. 2021), led us to study the methyl/ethyl (Me/Et) ratios in different molecular families in G+0.693 and other interstellar regions. In Fig. 4 we have compared the Me/Et ratio in G+0.693 with those found in the massive hot cores G31.41+0.31, Orion KL, and Sgr B2N, and the low-mass hot corino IRAS 16293-2422. We have considered the following different chemical families: alcohols (-OH), nitriles (-CN), formiates (-HCOO), thiols (-SH), and isocyanates (-NCO).

Figure 4 shows that in G+0.693, the observed ratio of MeNCO/EtNCO~8 is 2–4 times lower than the ratios for the formiates, alcohols, and thiols (32, 24, and 16, respectively) and ~4 times higher than the MeCN/EtCN ratio. Within each source, the Me/Et ratio of formiates, alcohols, and thiols falls within the same range considering the uncertainties. However, the Me/Et ratio is clearly lower in the N-bearing species: isocyanates (for which only the G+0.693 value is available) and nitriles. This suggests a more efficient production of EtNCO and EtCN, compared to their methyl-counterparts, than others ethyl derivatives.

4.3. Formation of C_2H_5NCO and H_2NCO^+ and in the ISM

The interstellar formation of the simplest isocyanates, HNCO and CH_3NCO, have been studied both theoretically (e.g., Quan et al. 2010; Cernicharo et al. 2016; Martín-Doménech et al. 2017; Quénard et al. 2018; Majumdar et al. 2018) and experimentally (Ligterink et al. 2017; Maté et al. 2018). However, little is known about EtNCO and H_2NCO^+.

Regarding EtNCO, there is no reaction proposed in the UMIST (McElroy et al. 2013) or KIDA (KInetic Database for Astrochemistry; Wakelam et al. 2012) chemical databases. Sewiło et al. (2019) propose the ion-molecule reaction in the gas phase $C_2H_5OH_2^+ + HNCO \rightarrow C_2H_5NCO + H_2O$. Despite the viability of the reaction, the abundance of a protonated species normally decreases by a few orders of magnitude with respect to the non-protonated one, as we have seen, for example, with H_2NCO^+ and HNCO towards G+0.693 (H_2NCO^+/HNCO~0.5×10^{-3}). Since the abundance of EtOH towards G+0.693 is $\sim5\times10^{-9}$ (Requena-Torres et al. 2006), the expected abundance of $C_2H_5OH_2^+$ would be of the order of 10^{-12}, which is below the derived abundance of EtNCO. Therefore, it seems unlikely that $C_2H_5OH_2^+$ would be a progenitor of EtNCO. Another possible formation pathway could involve analogous routes to that proposed for MeNCO. As discussed by Majumdar et al. (2018), MeNCO can be efficiently formed on the dust grains by the radical-radical reaction $CH_3 + NCO \rightarrow CH_3NCO$, which has also been proven experimentally (Ligterink et al. 2017). Therefore, the analogous grain surface reaction $C_2H_5 + NCO \rightarrow C_2H_5NCO$ might play an important role in the production of this species, although further experimental and/or theoretical work is needed to confirm this hypothesis.

Regarding H_2NCO^+, Marcelino et al. (2018) suggest the thermodynamically possible ion-molecule reaction $NH_3 + HCO^+ \rightarrow H_2NCO^+ + H_2$. This process is exothermic but clearly competes with the – probably – faster acid-base channel, that is $HCO^+ + NH_3 \rightarrow CO + NH_4^+$. Another possible reaction, proposed in the UMIST database, involves the ion-molecule reaction $HNCO^+ + H_2 \rightarrow H_2NCO^+ + H$. We note that $HNCO^+$ could be obtained by photoionisation (HNCO first ionisation potential ~11.60 eV; Holzmeier et al. 2015) through secondary photons since the cosmic-ray ionisation rate is high in the Galactic Centre (Goto 2013). A similar ion-molecule reaction was proposed by Iglesias (1977) with NCO^+ and H_2. However, none of these ions have been detected in the ISM to date. Alternative routes involve the gas phase proton transfer with a more acidic compound: $HNCO + HX^+ \rightarrow H_2NCO^+ + X$. The best candidate is H_3^+ due to its high abundance in the

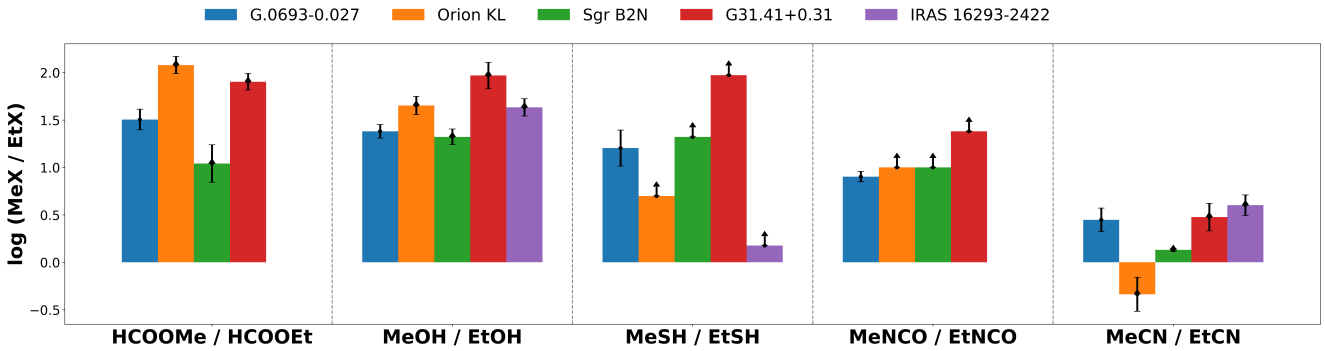

Fig. 4. Comparison of MeX/EtX ratios among different regions of the ISM, where X = HCOO, OH, SH, NCO, and CN (*from right to left*). The data have been taken from the following: Zeng et al. (2018), Rodríguez-Almeida et al. (2021), and this work for G+0.693-0.027; Kolesniková et al. (2014), López et al. (2014), Tercero et al. (2015), and Kolesniková et al. (2018) for Orion KL; Belloche et al. (2009) and Kolesniková et al. (2018) for Sgr B2N; Mininni et al. (2020), Colzi et al. (2021), and Mininni et al. (in prep.) for G31.41+0.31; and Drozdovskaya et al. (2019) for IRAS 16293-2422.

ISM (Oka 2006) and considering that its gas basicity is lower than HNCO (4.4 versus 7.8 eV, respectively; Hunter & Lias 1998). This reaction is also proposed in both KIDA and UMIST databases with a temperature-dependent reaction rate that decreases by a factor of ∼3 when the temperature goes from 10 K to 100 K, which could explain the differences seen in the H_2NCO^+/HNCO ratios towards L483 and G+0.693.

5. Conclusions

In this Letter, we report the detection of EtNCO (for the first time in the ISM) and H_2NCO^+ towards the molecular cloud G+0.693-0.027. We derived molecular abundances of $(6 \pm 2) \times 10^{-11}$ and $(1.3 \pm 0.5) \times 10^{-11}$, respectively. While the formation of EtNCO is more likely to proceed on the surface of dust grains, H_2NCO^+ is possibly formed via the proton exchange of H_3^+ with HNCO, as suggested by the change in the abundance ratio of H_2NCO^+/HNCO with temperature.

We have also studied the full inventory of the isocyanate family towards G+0.693. The relative abundance of HNCO:MeNCO:EtNCO is 1:1/55:1/447, which implies a decrease by a factor of 10 progressively going from HNCO to MeNCO and to EtNCO.

We have compared the Me/Et ratios among functional groups derived towards G+0.693 and several Galactic hot cores and corinos. Within each source, the values for the ratios of HCOOMe/HCOOEt and MeOH/EtOH are similar, which is also followed by the MeSH/EtSH ratio towards G+0.693. However, the Me/Et ratio for the N-bearing compounds (isocyanates and nitriles) are lower, which might indicate a more efficient production of their associated ethyl derivatives.

Acknowledgements. We are grateful to the IRAM 30m and Yebes 40m telescope staff for help during the different observing runs. IRAM is supported by the National Institute for Universe Sciences and Astronomy/National Center for Scientific Research (France), Max Planck Society for the Advancement of Science (Germany), and the National Geographic Institute (IGN) (Spain). The 40m radio telescope at Yebes Observatory is operated by the IGN, Ministerio de Transportes, Movilidad y Agenda Urbana. L. F. R.-A., V. M. R. and L. C. acknowledge support from the Comunidad de Madrid through the Atracción de Talento Investigador Modalidad 1 (Doctores con experiencia) Grant (COOL:Cosmic Origins of Life; 2019-T1/TIC-15379). I. J.-S. and J. M.-P. have received partial support from the Spanish State Research Agency (AEI) project number PID2019-105552RB-C41. We also acknowledge support from the Spanish National Research Council (CSIC) through the i-Link project number LINKA20353. P. dV. and B. T. thank the support from the European Research Council through Synergy Grant ERC-2013-SyG, G.A. 610256 (NANOCOSMOS) and from the Spanish Ministerio de Ciencia e Innovación (MICIU) through project PID2019-107115GB-C21. B. T. also thanks the Spanish MICIU for funding support from grant PID2019-106235GB-I00.

References

Agúndez, M., Marcelino, N., Cernicharo, J., Roueff, E., & Tafalla, M. 2019, A&A, 625, A147
Belloche, A., Garrod, R., Müller, H., et al. 2009, A&A, 499, 215
Bouchy, A., & Roussy, G. 1977, J. Mol. Spectr., 68, 156
Bouchy, A., & Roussy, G. 1979, J. Mol. Spectr., 77, 145
Cernicharo, J., Kisiel, Z., Tercero, B., et al. 2016, A&A, 587, L4
Choe, J. C. 2021, ApJ, 914, 136
Colzi, L., Rivilla, V. M., Beltrán, M. T., et al. 2021, A&A, 653, A129
Drozdovskaya, M. N., van Dishoeck, E. F., Rubin, M., Jørgensen, J. K., & Altwegg, K. 2019, MNRAS, 490, 50
Fontani, F., Colzi, L., Redaelli, E., Sipilä, O., & Caselli, P. 2021, A&A, 651, A94
Gorai, P., Bhat, B., Sil, M., et al. 2020, ApJ, 895, 86
Goto, M. 2013, Proc. Int. Astron. Union, 9, 429
Gupta, H., Gottlieb, C., Lattanzi, V., Pearson, J., & McCarthy, M. 2013, ApJ, 778, L1
Halfen, D., Ilyushin, V. V., & Ziurys, L. M. 2015, ApJ, 812, L5
Heineking, N., Grabow, J.-U., & Stahl, W. 1994, Mol. Phys., 81, 1177
Hocking, W., & Gerry, M. 1976, J. Mol. Spectr., 59, 338
Holzmeier, F., Lang, M., Fischer, I., et al. 2015, J. Chem. Phys., 142, 184306
Hunter, E. P., & Lias, S. G. 1998, J. Phys. Chem. Ref. Data, 27, 413
Iglesias, E. 1977, ApJ, 218, 697
Jiménez-Serra, I., Martín-Pintado, J., Rivilla, V. M., et al. 2020, Astrobiology, 20, 1048
Kawaguchi, K., Saito, S., & Hirota, E. 1985, Mol. Phys., 55, 341
Kirby, C., & Kroto, H. 1978, J. Mol. Spectr., 70, 216
Kolesniková, L., Tercero, B., Cernicharo, J., et al. 2014, ApJ, 784, L7
Kolesniková, L., Alonso, E., Tercero, B., Cernicharo, J., & Alonso, J. 2018, A&A, 616, A173
Lattanzi, V., Thorwirth, S., Gottlieb, C. A., & McCarthy, M. C. 2012, J. Phys. Chem. Lett., 3, 3420
Ligterink, N., Coutens, A., Kofman, V., et al. 2017, MNRAS, 469, 2219
Ligterink, N., Ahmadi, A., Coutens, A., et al. 2021, A&A, 647, A87
López, A., Tercero, B., Kisiel, Z., et al. 2014, A&A, 572, A44
Majumdar, L., Loison, J.-C., Ruaud, M., et al. 2018, MNRAS, 473, L59
Marcelino, N., Agúndez, M., Cernicharo, J., Roueff, E., & Tafalla, M. 2018, A&A, 612, L10
Martín, S., Requena-Torres, M., Martín-Pintado, J., & Mauersberger, R. 2008, ApJ, 678, 245
Martín, S., Martín-Pintado, J., Blanco-Sánchez, C., et al. 2019, A&A, 631, A159
Martín-Doménech, R., Rivilla, V., Jiménez-Serra, I., et al. 2017, MNRAS, 469, 2230
Maté, B., Molpeceres, G., Tanarro, I., et al. 2018, ApJ, 861, 61
McElroy, D., Walsh, C., Markwick, A., et al. 2013, A&A, 550, A36
Mininni, C., Beltrán, M., Rivilla, V., et al. 2020, A&A, 644, A84
Oka, T. 2006, PNAS, 103, 12235
Pascal, R., Boiteau, L., & Commeyras, A. 2005, Top. Curr. Chem., 259, 69
Quan, D., Herbst, E., Osamura, Y., & Roueff, E. 2010, ApJ, 725, 2101
Quénard, D., Vastel, C., Ceccarelli, C., et al. 2017, MNRAS, 470, 3194

Quénard, D., Jiménez-Serra, I., Viti, S., Holdship, J., & Coutens, A. 2018, MNRAS, 474, 2796
Requena-Torres, M., Martín-Pintado, J., Rodríguez-Franco, A., et al. 2006, A&A, 455, 971
Requena-Torres, M., Martín-Pintado, J., Martín, S., & Morris, M. 2008, ApJ, 672, 352
Rivilla, V., Martín-Pintado, J., Jiménez-Serra, I., et al. 2019, MNRAS, 483, L114
Rivilla, V. M., Martín-Pintado, J., Jiménez-Serra, I., et al. 2020, ApJ, 899, L28
Rivilla, V. M., Jiménez-Serra, I., Martín-Pintado, J., et al. 2021a, PNAS, 118
Rivilla, V., Jiménez-Serra, I., García de la Concepción, J., et al. 2021b, MNRAS, 506, L79
Rodríguez-Almeida, L. F., Jiménez-Serra, I., Rivilla, V. M., et al. 2021, ApJ, 912, L11
Ross, S. C., Cooper, T. A., Firth, S., Kroto, H. W., & Walton, D. R. 1992, J. Mol. Spectr., 152, 152
Saito, S., & Amano, T. 1970, J. Mol. Spectr., 34, 383
Sakaizumi, T., Yamada, O., Ushida, K., Ohashi, O., & Yamaguchi, I. 1976, Bull. Chem. Soc. Jpn., 49, 2908
Schneider, C., Becker, S., Okamura, H., et al. 2018, Angew. Chem., 57, 5943
Sewiło, M., Charnley, S. B., Schilke, P., et al. 2019, ACS Earth Space Chem., 3, 2088
Snyder, L. E., & Buhl, D. 1972, ApJ, 177, 619
Tercero, B., Cernicharo, J., López, A., et al. 2015, A&A, 582, L1
Tercero, F., López-Pérez, J., Gallego, J., et al. 2021, A&A, 645, A37
Wakelam, V., Herbst, E., Loison, J.-C., et al. 2012, ApJS, 199, 21
Zeng, S., Jiménez-Serra, I., Rivilla, V., et al. 2018, MNRAS, 478, 2962
Zeng, S., Zhang, Q., Jiménez-Serra, I., et al. 2020, MNRAS, 497, 4896
Zeng, S., Jiménez-Serra, I., & Rivilla, V. 2021, A&A, Submitted

Appendix A: Spectroscopic information of the isocyanates searched towards G+0.693

In Table A.1 we have introduced all the molecules searched for in our spectral survey. The pertinent references for the line list and dipole moments are included for each one.

For EtNCO, the spectral predictions were done by re-evaluating the ro-vibrational partition function in a similar way as with MeNCO by Cernicharo et al. (2016), who only accounted for the vibrational states below 2.6 GHz. For more details, readers can refer to Colzi et al. 2021 (Appendix B.2).

Table A.1. Spectroscopic information and references for the molecules studied in this work.

Molecule	Catalogue	Tag	Dipole moment	Line list
C_2H_5NCO	MADCUBA[a]	...	Sakaizumi et al. (1976)	Heineking et al. (1994), Kolesniková et al. (2018)
H_2NCO^+	CDMS	044516	Lattanzi et al. (2012)	Gupta et al. (2013)
NCO	CDMS	042503	Saito & Amano (1970)	Kawaguchi et al. (1985)
cis-C_2H_3NCO	MADCUBA[a]	...	Bouchy & Roussy (1977)	Kirby & Kroto (1978)
trans-C_2H_3NCO	MADCUBA[a]	...	Bouchy & Roussy (1977, 1979)	Kirby & Kroto (1978)
NCNCO	MADCUBA[a]	...	Hocking & Gerry (1976)	Hocking & Gerry (1976)
HCCNCO	MADCUBA[a]	...	Assumed[b]	Ross et al. (1992)

Notes. [a]The entry was imported into MADCUBA using the spectroscopic works listed in the table. [b]Since there is no value reported in the literature, the *.cat file was generated assuming $\mu_a = 1.0$ D.

Appendix B: Observed transitions and line parameters derived from the LTE fit of H_2NCO^+

In Table B.1 we have listed the complete description of the lines of H_2NCO^+ plotted in Figure 1. The transition of o-H_2NCO^+ at 100.307 GHz ($5_{1,5} - 4_{1,4}$, $E_u = 13.5$ K) is not shown, and it has not been considered for the fit because it is heavily blended with CH_3OCHO (line at 100.308 GHz; intensity ~ 60 mK versus ~ 7 mK for H_2NCO^+).

It is important to note that both ortho and para H_2NCO^+ CDMS entries incorporate the ^{14}N nuclear spin hyper-fine splitting, but in our data these lines are unresolved. Hence, for simplicity, the F quantum numbers have been omitted from Figure 2 (see Table B.1 for a complete description of the lines and quantum numbers).

Table B.1. Spectroscopic and information of the LTE fitting of the selected lines of o-H_2NCO^+ and p-H_2NCO^+ shown in Figure 2. The frequency, the QNs, the energy of the upper level (E_u), the logarithm of the intensity (at 300 K), $\int T_A^* d\nu$, and the S/N in integrated intensity of the lines are given.

Molecule	Frequency (GHz)	QNs[a]	E_u (K)	log Intensity (nm^2 MHz)	$\int T_A^* d\nu$[b] (K km s^{-1})	S/N[b]
o-H_2NCO^+	40.122511	$2_{1,2}$-$1_{1,1}$ F = 1- 1	1.9	-5.0506	0.194	23
	40.122797	$2_{1,2}$-$1_{1,1}$ F = 1- 2	1.9	-6.2267	...	...
	40.123224	$2_{1,2}$-$1_{1,1}$ F = 1 - 0	1.9	-4.9256	...	...
	40.123539	$2_{1,2}$-$1_{1,1}$ F = 3 - 2	1.9	-4.3024	...	...
	40.124590	$2_{1,2}$-$1_{1,1}$ F = 2 - 1	1.9	-4.5734	...	...
	40.124876	$2_{1,2}$-$1_{1,1}$ F = 2 - 2	1.9	-5.0505	...	...
	40.781503	$2_{1,1}$-$1_{1,0}$ F = 1 - 0	2.0	-4.9115	0.116	17
	40.782899	$2_{1,1}$-$1_{1,0}$ F = 2 - 2	2.0	-5.0364	...	...
	40.783205	$2_{1,1}$-$1_{1,0}$ F = 3 - 2	2.0	-4.2882	...	...
	40.784147	$2_{1,1}$-$1_{1,0}$ F = 2 - 1	2.0	-4.5593	...	...
	40.784622	$2_{1,1}$-$1_{1,0}$ F = 1 - 1	2.0	-5.0364	...	...
	80.246416	$4_{1,4}$-$3_{1,3}$ F = 5 - 4	8.7	-3.3697	0.211	31
	80.246532	$4_{1,4}$-$3_{1,3}$ F = 3 - 2	8.7	-3.6030	...	...
	80.246564	$4_{1,4}$-$3_{1,3}$ F = 4 - 3	8.7	-3.4849	...	...
	81.565492	$4_{1,3}$-$3_{1,2}$ F = 3 - 2	8.8	-3.5890	0.209	31
	81.565524	$4_{1,3}$-$3_{1,2}$ F = 5 - 4	8.8	-3.3557	...	...
	81.565633	$4_{1,3}$-$3_{1,2}$ F = 4 - 3	8.8	-3.4709	...	...
	101.95584	$5_{1,4}$-$4_{1,3}$ F = 4 - 3	13.7	-3.0757	0.165	18
	101.95585	$5_{1,4}$-$4_{1,3}$ F = 6 - 5	13.7	-3.1660	...	...
	101.95591	$5_{1,4}$-$4_{1,3}$ F = 5 - 4	13.7	-4.5462	...	...
p-H_2NCO^+	40.453210	$2_{0,2}$-$1_{0,1}$ F = 1 - 0	2.9	-4.8970	0.168	20
	40.454746	$2_{0,2}$-$1_{0,1}$ F = 3 - 2	2.9	-4.1488	...	...
	40.454815	$2_{0,2}$-$1_{0,1}$ F = 2 - 1	2.9	-4.4199	...	...
	40.455616	$2_{0,2}$-$1_{0,1}$ F = 1 - 0	2.9	-4.7720	...	...
	40.455778	$2_{0,2}$-$1_{0,1}$ F = 2 - 2	2.9	-4.8970	...	...
	80.906908	$4_{0,4}$-$3_{0,3}$ F = 5 - 4	9.7	-3.3131	0.261	
	80.906934	$4_{0,4}$-$3_{0,3}$ F = 4 - 3	9.7	-3.4283	...	...
	80.907001	$4_{0,4}$-$3_{0,3}$ F = 3 - 2	9.7	-3.5464	...	...
	101.13112	$5_{0,5}$-$4_{0,4}$ F = 6 - 5	14.6	-3.0434	0.213	
	101.13114	$5_{0,5}$-$4_{0,4}$ F = 5 - 4	14.6	-3.1336	...	...
	101.13117	$5_{0,5}$-$4_{0,4}$ F = 4 - 3	14.6	-3.2251	...	...
	101.13223	$5_{0,5}$-$4_{0,4}$ F = 5 - 5	14.6	-4.5138	...	...

Notes. [a]The CDMS entry accounts for the hyper-fine splitting because of the nuclear spin of ^{14}N. Hence the QNs are presented in this way: $J''_{K''_a,K''_c} \rightarrow J'_{K'_a,K'_c}$ F = F'' → F'. [b]In our data, the hyper-fine splitting is unresolved. Thus, the S/N was calculated by the sum of the individual F'' → F' components.

Appendix C: Selected lines for computing the upper limits

In Table C.1 we have listed the brightest and cleanest lines for the column density upper limit determination for the non-detected isocyanates. Namely: NCO, cis- and trans-C_2H_3NCO, and NCNCO.

Table C.1. Lines employed to compute the upper limits to the column density of the isocyanates that have not been detected towards G+0.693.

Molecule	Frequency (GHz)	QNs	E_u (K)	$\int T_A^* dv$ (mK km s^{-1})	N (cm^{-2})
NCO ($^2\Pi_{3/2}$)	81.404300	7/2 – 5/2 F = 9/2 – 7/2 e	6.7	25	$<1.4\times10^{13}$
	81.404813	7/2 – 5/2 F = 9/2 – 7/2 f	6.7	25	...
c-C_2H_3NCO	46.281730	$8_{2,7}$-$7_{2,6}$	13.1	46	$<9.3\times10^{12}$
t-C_2H_3NCO	33.483408	$7_{0,7}$-$6_{0,6}$	6.4	21	$<2.5\times10^{12}$
NCNCO	42.364035	$8_{0,8}$-$7_{0,7}$	9.2	19	$<1.2\times10^{12}$
HCCNCO	35.291156	$7_{0,7}$-$6_{0,6}$	7.1	28	$<8.9\times10^{12}$

Appendix D: Molecular abundances of the isocyanates searched towards G+0.693

In Table D.1 we list the values of the molecular abundances of the isocyanates studied in this work with respect to H_2, which are plotted in Figure 3. Additionally, we have also included the values of the column density together with the errors derived from the LTE fit with MADCUBA. The uncertainties of the molecular abundances consider the errors derived from the column density and an additional 15% consider the calibration errors.

Table D.1. Molecular abundance ratios of the isocyanates searched towards G+0.693.

Molecule	$N_X \pm \Delta N_X$ ($\times10^{13}$ cm^{-2})	N_x/N_{H_2}
NCO	<1.4	$<1.0\times10^{-10}$
HNCO [(a)]	$(3.6\pm0.1)\times10^{2}$	$(2.3–3.1)\times10^{-8}$
o-H_2NCO^+	1.1 ± 0.2	$(5.8–9.8)\times10^{-12}$
p-H_2NCO^+	$(6.3\pm1.7)\times10^{-2}$	$(3.3–6.1)\times10^{-12}$
(o+p)-H_2NCO^+	$(1.7\pm0.2)\times10^{-1}$	$(1.1–1.5)\times10^{-11}$
NCNCO	<0.12	$<8.7\times10^{-12}$
CH_3NCO [(a)]	6.6 ± 0.4	$(4.1–5.7)\times10^{-10}$
C_2H_5NCO	8.1 ± 1.3	$(4.7\pm7.3)\times10^{-11}$
trans-C_2H_3NCO	<0.25	$<1.8\times10^{-11}$
cis-C_2H_3NCO	<0.93	$<6.9\times10^{-11}$
HCCNCO	<0.89	$<6.6\times10^{-11}$

Notes. [(a)]Data taken from Zeng et al. (2018).